

# Scanning tunneling spectroscopy of cleaved InAs/GaAs quantum dots at low temperatures

A. Urbieto,<sup>1,4</sup> B. Grandidier,<sup>1</sup> J. P. Nys,<sup>1</sup> D. Deresmes,<sup>1</sup> D. Stiévenard,<sup>1</sup> A. Lemaître,<sup>2</sup> G. Patriarche,<sup>2</sup> and Y. M. Niquet<sup>3</sup>

<sup>1</sup>Département ISEN, Institut d'Electronique de Microélectronique et de Nanotechnologie (IEMN), CNRS, UMR 8520, 41 Boulevard Vauban, 59046 Lille Cedex, France

<sup>2</sup>CNRS-Laboratoire de Photonique et de Nanostructures, Route de Nozay, 91460 Marcoussis, France

<sup>3</sup>CEA Grenoble, INAC/SP2M/L Sim, 17 Rue des Martyrs, 38054 Grenoble Cedex 9, France

<sup>4</sup>Departamento de Física de Materiales, Universidad Complutense de Madrid, 28040 Madrid, Spain

(Received 25 October 2007; revised manuscript received 25 February 2008; published 9 April 2008)

We investigate the electronic structure of cleaved InAs quantum dots that are embedded in GaAs by means of scanning tunneling spectroscopy at low temperatures. By using a structure containing arrays of quantum dots surrounded by *p*-type buffer layers, spatial mapping of the empty states shows the electronic structure of the conduction band states and reveals states lying at lower energy with an interfacial localization at the top of the dot. From the knowledge of the structural properties of the dots that are obtained from transmission electron microscopy experiments, tight-binding calculations of the electronic structure of cleaved dots are performed. The observed square of the wave functions for the different states are compared to the ones that are obtained by the tight-binding calculations.

DOI: [10.1103/PhysRevB.77.155313](https://doi.org/10.1103/PhysRevB.77.155313)

PACS number(s): 73.21.La, 68.65.-k, 68.37.Ef

## I. INTRODUCTION

Semiconductor quantum dots (QDs) allow access to rich physical phenomena due to their atomlike properties and have become crucial for a wide range of technological applications.<sup>1,2</sup> Engineering optical quantum devices requires a precise control of the QD oscillator strength, which is directly related to their electronic structure and thus depends on the structural properties of the QDs, such as their size, shape, composition, and strain. Among the existing semiconductor QDs, self-assembled semiconductor QDs result from the spontaneous growth of a highly lattice mismatched semiconductor layer onto another semiconductor layer. The latter material is also used during the overgrowth of the QDs.<sup>3</sup> Such a capping precludes from a detailed knowledge of the QD structural properties and therefore spectroscopic studies are greatly needed to determine the carrier localization in the QDs.

In the most common self-assembled QDs, for example, InAs QDs that are embedded in a GaAs matrix material, the electron confining potential is high enough to keep the electron localized in the center of the dot. However, questions still arise as to the hole localization. By measuring the photocurrent out of an InAs QD under an electric field, Fry *et al.*<sup>4</sup> found a permanent dipole moment, which indicated that the hole wave function was not localized in the center of the dot. Such a result stimulated numerous theoretical works, which now take into account many structural parameters of the dots.<sup>5</sup> For QDs with lattice mismatched components different from InAs/GaAs, an interfacial hole localization has been predicted, but experimental evidences are still lacking.<sup>6</sup>

In contrast to optical spectroscopic techniques,<sup>7</sup> electrical spectroscopic techniques, such as *C-V* spectroscopy or tunneling spectroscopy, provide a direct method to probe the discrete electronic structure of QDs and have offered the unique advantage to spatially map out the square of the electron wave functions.<sup>8-12</sup> Although the hole states are generally less confined in these systems, magnetocapacitance

spectroscopy has recently proved to be successful to resolve the *k*-space wave functions in the valence band.<sup>13,14</sup> For most of the dots which have been investigated, the symmetry of the electron and hole wave functions was obtained in a plane that is parallel to the base of the dots. Such analysis has made possible a detailed understanding of the variations that are observed in the symmetry of the wave functions for dots with different geometries, such as InAs QDs grown on different oriented substrates.<sup>15</sup> However, since the confinement is stronger in the direction perpendicular to the QD base, a direct measurement of the dipole moment for individual dots requires us to probe the extent of the electron and hole wave functions along the growth direction.

Here, we investigate the electronic transport in cleaved self-assembled InAs QDs, which are embedded in GaAs, by using scanning tunneling spectroscopy (STS) at low temperatures. By using *p*-type buffer layers surrounding the arrays of QDs, we are able to probe not only the conduction band states of the QDs but also the empty states lying below the bottom of the conduction band. By calculating the single particle electronic structure of a cleaved dot, which is based on a precise knowledge of its shape and composition from dark field (DF) images, which are obtained in transmission electron microscopy (TEM), we show that the conductance images of the electron states are in good agreement with the predictive theoretical modeling of the electron wave function. The situation is more complicated for the empty states that are positioned below the bottom of the conduction band. Although these states should arise from the contribution of valence band states of the QDs due to the upward tip induced band bending, the experimental observations reveal a striking interfacial localization, which is not predicted by theoretical calculations.

## II. EXPERIMENTAL RESULTS

The samples were grown by molecular beam epitaxy and are made of six arrays of QDs that are separated by 15 nm

GaAs spacers. Such a spacer thickness allows the self-organization of QDs into columns along the growth direction with a limited lateral strain in the overlayer so that the QDs have similar lateral sizes in the column.<sup>16,17</sup> The array was surrounded by an InGaAs layer used as a marker and then a 300 nm thick *p*-type GaAs buffer layer with a concentration of  $2.0 \times 10^{19}$  Be cm<sup>-3</sup> on both side. By using such highly *p*-doped GaAs buffers, we are able to adjust the Fermi level in the semiconductor so that it is positioned less than 50 meV above the top of the QD valence band when no electric field is applied in the semiconductor. The samples were cleaved in an ultrahigh vacuum system with a low temperature scanning tunneling microscopy (STM).<sup>18</sup> In order to perform spectroscopic measurements, maps of the differential conductance were recorded with a lock-in amplifier ( $V_{\text{mod}}=7$  meV and  $f_{\text{mod}}=1$  kHz). The composition distribution in the QD was determined from the analysis of the intensity variations in TEM 002 DF images, where  $\langle 110 \rangle$  cross-sectional thin foils with a thickness of 10–12 nm were prepared, as described elsewhere.<sup>19</sup>

Figure 1(a) shows a constant current height image of four QD arrays (parallel bright layers in the right part of the figure) with the lowest bright InGaAs marker of the structure (left part). Bright protrusions are also seen in the arrays and correspond to individual QDs. The QDs are either found isolated or self-organized into a column. In this latter case, the dots are generally not well aligned, as shown in Fig. 1(a), which is consistent with a limited lateral strain in the overgrowth layer due to the GaAs spacer layer thickness of 15 nm.<sup>16</sup> From the high resolution images, such as the one visible in the inset of Fig. 1(a), we observe that the dots have a lens shape with a base length of  $17 \pm 3$  nm and a height generally varying between seven and nine atomic rows, which include the wetting layer.

Typical spectroscopic measurements, which are averaged in the center of the dots and acquired at  $T=77$  K with a variable tip-sample distance for higher measurement sensitivity,<sup>20</sup> are shown in Fig. 1(b). The Fermi level  $E_F$  is positioned at 0 V above the top of the valence band, which is observed for negative voltages. At positive voltages, a shoulder is first obtained, which is followed by a succession of peaks. We attribute the three peaks to the quantized conduction band states of the QD. The onset observed at higher voltage may arise from the first electron subband of the wetting layer.

Turning now to the shoulder that is observed between +0.5 and +1.2 eV, we know that the Fermi level lies much closer to the valence band of the QD than to the conduction band due to the insertion of degenerated *p*-type GaAs buffer layers at each side of the QD structure. At low positive sample voltages, the tip induces an upward band bending,<sup>21</sup> which makes the valence band states of the QDs empty. Therefore, those states contribute to the tunnel current before the tip Fermi level becomes aligned with the QD conduction band states [see the inset of Fig. 1(b)]. As the hole levels are generally less spaced than the electron levels in InAs/GaAs QDs,<sup>22,23</sup> they are likely to yield a broad shoulder instead of a series of peaks at  $T=77$  K.

By comparing the spectrum measured at 77 K with the spectrum measured at 5 K, we first note that the electron

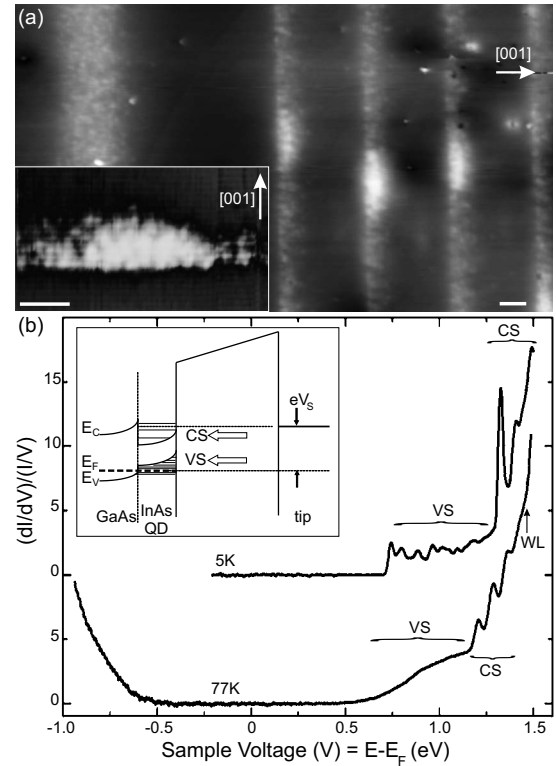


FIG. 1. (a) Cross-sectional STM image showing arrays of InAs QDs and an InGaAs quantum well marker in GaAs. Inset: High resolution STM images of a QD. A high pass filtering has been performed to highlight the atomic rows. The images were acquired at a sample voltage  $V_s$  of  $-1.5$  V, a tunneling current of 80 pA, and a temperature of 77 K. (b) Tunneling spectra acquired in the center of a cleaved QD with variable tip-sample distances at two different temperatures. The empty valence band states caused by the tip induced band bending and the conduction band states are labeled as VS and CS, respectively. The position of the wetting layer is indicated by an arrow. Inset: Band diagram showing the QDs states that contribute to the tunneling current at a positive energy  $eV_s$  with respect to the sample Fermi level  $E_F$ .

states of the QDs are shifted to higher energies, which indicate a reduced screening in the sample close to the cleaved surface. Such a result is consistent with other STS studies, which are performed on semiconductor surfaces, where the band edges are shifted to higher energies at low temperature due to the transport limitations in the semiconductor.<sup>24,25</sup> Then, peaks appear in the energy range where the shoulder was seen at  $T=77$  K. When we compare the peak separations, we find that the energy separation between the two lowest electron states (80 meV) is quite comparable to the separation that is measured between some of these peaks, for example, between the second (+0.80 V) and third (+0.88 V) peaks or the third and fourth (+0.96 V) peaks.

To gain more insight into the electronic structure of the QD at  $T=5$  K, spatially resolved spectroscopic measurements were acquired at constant tip-sample distance and were shown in Fig. 2. For each peak that is observed in the tunneling spectra, which is measured at different locations of a dot [Fig. 2(a)], we display the differential conductance images [Fig. 2(b)]. Focusing first on the strongest peak posi-

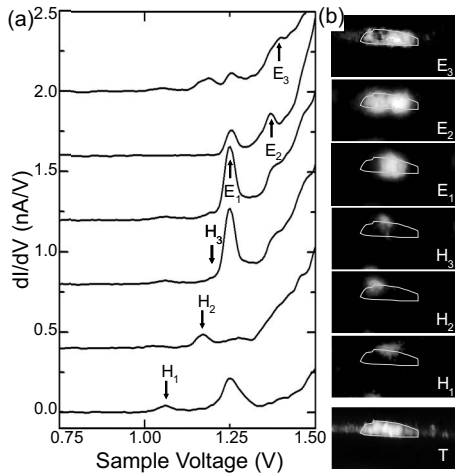


FIG. 2. (a) Spatially resolved tunneling spectroscopic measurements acquired in different regions of a QD at 5 K. (b) Differential conductivity images that were obtained for the same QD, as shown in the topographic image ( $T$ ), with its boundaries outlined by a white line. The spectra correspond to the averaged  $dI/dV$  curves that were acquired in the regions of the  $dI/dV$  images that were bright at the energies indicated by an arrow. The feedback parameters were  $V_s = +1.9$  V and  $I_{\text{stab}} = 600$  pA.

tioned at the energy  $E_1 = 1.25$  eV, the spatial map of the differential conductance shows a simple lobe centered in the dot and extending from the bottom to the top of the dot [Fig. 2(b), map  $E_1$ ]. The next peak, at an energy of  $E_2 = 1.36$  eV, corresponds to a feature with two lobes, which are localized in the whole dot with a node in the center of the dot [Fig. 2(b), map  $E_2$ ]. From the symmetry of the features that are resolved at the energies  $E_1$  and  $E_2$ , which show a spatial contrast resembling the square of an  $s$ -like wave function and a  $p$ -like wave function, respectively, we attribute the peaks at the energies  $E_1$  and  $E_2$  to the tunneling of electrons through the ground state and the first excited state of the conduction band in the dot. Finally, we obtain a third peak at higher energy ( $E_3 = 1.40$  eV), which should correspond to the second electron excited state in the dot [Fig. 2(b), map  $E_3$ ].

For the dot shown in Fig. 2, we are able to resolve the three states below the electron ground state. The states are labeled as  $H_1$ ,  $H_2$ , and  $H_3$  and lie at energies of 1.06, 1.17, and 1.20 eV, respectively. From the conductance image, as shown in Fig. 2(b), it is clear that these states extend much less than the electron wave functions. Surprisingly, all three states are not localized in the dot but at the top interface of the dot.

To statistically get relevant information on the hole localization in the InAs QD for the ground state, other dots were investigated in a similar way at temperatures of 5 and 77 K. Figure 3 shows two other examples of topographic image of dots as well as their respective conductance maps for the electron ground state and the first state contributing to the tunneling current at positive bias. Again, by highlighting the contour of the dots in Figs. 3(a) and 3(b), it is clear that this state has an interfacial localization, having only a small overlap with the electron ground state.

In InAs QDs embedded in GaAs, the confining potential is generally much lower for the hole states than that for the

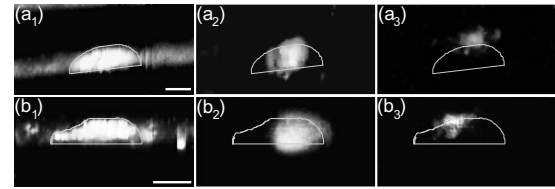


FIG. 3. (a<sub>1</sub>) and (b<sub>1</sub>) topographic STM images of the two QDs ( $V_s = +1.60/+2.00$  V) and the respective maps of the differential conductivities for the electron ground states (a<sub>2</sub>) and (b<sub>2</sub>) ( $V_s = +1.25/+1.36$  V) and the first lowest state that contribute to the current at positive biases (a<sub>3</sub>) and (b<sub>3</sub>) ( $V_s = +0.94/+1.00$  V). The boundaries of the dots are outlined by a white line. The bar scale corresponds to 5 nm.

electron states.<sup>26</sup> Since variations of the chemical composition and strain in the dot modify the confining potential, the localization of the holes depends in a critical way on the structural properties of the dot.<sup>27,28</sup> As a result, the chemical composition of the dot must be known to identify the origin of the hole localization.

In order to get a quantitative measurement of the In composition of the dots, we performed cross-sectional 002 DF TEM images of the QDs in the array, as shown in the inset of Fig. 4(a). While In compositions between  $x = 0.1$  and 0.3 in  $\text{In}_x\text{Ga}_{1-x}\text{As}$  alloys give a contrast similar to the GaAs spacer, a bright contrast indicates an In concentration of more than 30% in the core of the QD.<sup>19</sup> Conversely, a dark contrast corresponds to an In concentration of less than 10% in the wetting layer. Based on the calibration of the contrast from  $\text{In}_x\text{Ga}_{1-x}\text{As}$  layers containing a wide range of In concentration, we measure the composition profile along the growth

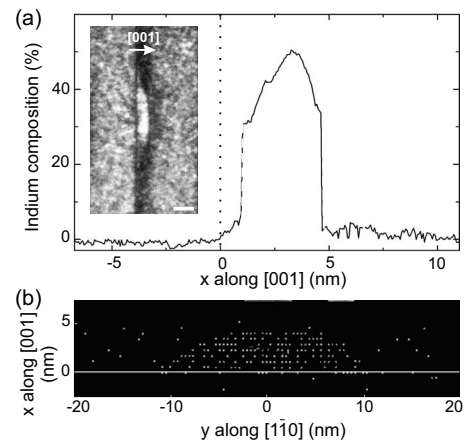


FIG. 4. (a) Indium composition profile that are obtained along the growth direction from 002 DF TEM images. The In profile is measured through the center of the dot and averaged laterally over a 4 nm segment. The dashed lines are used in regions of the QD, where the variation of the In concentration is abrupt. The vertical dotted line that is positioned at zero indicates the base of the QD. Inset: Cross-sectional 002 TEM dark field image of a QD (bar scale of 5 nm). (b) In atomic positions in the cleavage plane of a quantum dot used to calculate the electronic structure of the dot. The In concentration along the [001] direction corresponds to the one experimentally obtained from the TEM experiments. The QD base is indicated by a horizontal white line.

direction through the center of the dot, as shown in Fig. 4(a).

Such a profile reveals that the QD does not consist of a pure InAs core; instead, the In concentration gradually increases toward the top of the QD, then decreases more abruptly, which is consistent with a previous observation of other InAs QDs embedded in GaAs and analyzed by this method.<sup>19</sup> Taking into account the underestimation of the In concentration at the top due to the average measurement through the thickness of the foil, we find a maximum In concentration between 55% and 60%; the region with the highest In concentration is slightly shifted toward the top of the dots.

### III. THEORETICAL RESULTS

Knowing the In composition, we can perform numerical simulations to determine the strain distribution in the QDs and subsequently their electronic structure. The simulated dots have a lens shape with a diameter of  $\sim 20$  nm and a height of 5 nm, which correspond to the eight atomic rows that are observed in the STM images of the cleaved dots along the growth direction. The indium concentration in the dot follows the profile found by the TEM experiments along the [001] direction. Both fully embedded and cleaved dots were calculated for comparison. In the former case, periodic boundary conditions are applied in all directions, the layers of dots are separated by 15 nm along [001], and the dots are 40 nm apart in each layer. The dots are cleaved in the (110) plane running through their center. The dangling bonds on the cleaved surface and backplane (located 50 nm behind the cleaved surface) are saturated with hydrogen atoms. Strain relaxation in the fully embedded and cleaved QDs was calculated with Keating's valence force field model (1 334 372 atoms). The electronic structure of the dots was then calculated with a first nearest neighbor  $sp^3d^5s^*$  tight-binding model by taking the spin orbit and strains into account.<sup>29</sup>

Figures 5(a) and 5(b) show the square of the first electron and hole wave functions in the (110) plane of a cleaved dot and of a fully embedded dot, respectively. In the embedded dot, the second ( $E_2$ ) and third ( $E_3$ ) electron energy levels correspond to  $p$ -like states.  $E_3$  actually has a nodal plane in the (110) plane running through the center of the dot and is therefore hardly visible in Fig. 5(b). The  $E_2$  and  $E_3$  levels are not degenerate because the [110] and  $[1\bar{1}0]$  directions are not equivalent at the atomic scale (even for a pure InAs QD).<sup>26,28</sup> In the cleaved QD, only  $E_2$  still shows a clear  $p$ -like symmetry;  $E_3$  is already significantly coupled to the nearby wetting layer. Moreover, the strain relaxation in the cleaved QDs digs a well that tends to attract the lowest-lying electron wave functions toward the surface, as already discussed in Ref. 9. As for the holes, we find many more bound levels than the four ones, as displayed in Fig. 5. We note that the separation between the energy levels is much lower for the holes than that for the electrons due to a smaller confinement, as shown in Table I. Since the confinement of the holes strongly depends on the valence band offsets and deformation potentials, the calculations were repeated with different sets of parameters<sup>28,30</sup> (including, in particular, both positive and negative hydrostatic valence band deformation potentials

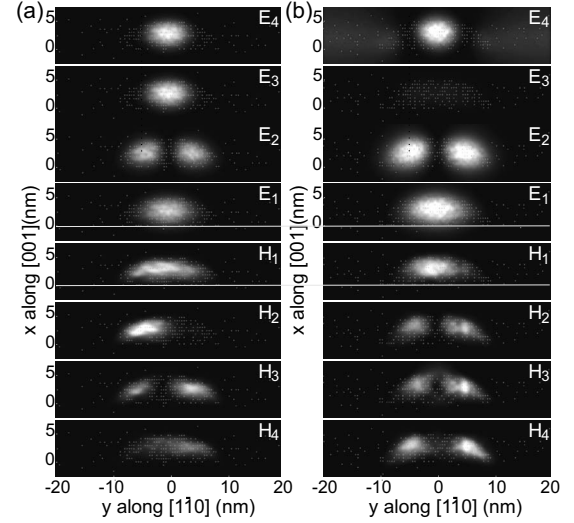


FIG. 5. Isodensity surfaces of the electron states  $E_i$  and hole states  $H_i$  that are plotted (a) in the (110) surface plane of a cleaved InAs quantum dot and (b) in the (110) plane running through the center of an embedded quantum dot. The In atoms in this plane appear as bright dots; their distribution is given in Fig. 4(b). The position of QD base is indicated by a white line for the electron and hole ground states. The results are obtained with the valence band offset and deformation potentials of Ref. 30.

$a_v$ ). However, the lowest-lying hole states are always found localized in the dot whatever the deformation potentials. Piezoelectric effects have also been considered but were unable to induce a significant shift of the hole state localization toward the interface of the dot.<sup>5</sup>

### IV. DISCUSSION

A comparison of the experimental data with the theoretical calculations shows a good agreement for the single particle electron states in the conduction band of the dots. We observe that the ground state and the first excited state are localized in the dots, with the expected  $s$ -like and  $p$ -like

TABLE I. Calculated single-particle electron ( $E_i$ ) and hole ( $H_i$ ) energy levels in a cleaved dot and in an embedded dot with the In distribution obtained from the TEM experiments. The energy levels are given with respect to the top of the bulk InAs valence band.

States	Energy levels (eV) (cleaved dot)	Energy levels (eV) (embedded dot)
$E_4$	1.310	1.305
$E_3$	1.300	1.289
$E_2$	1.292	1.285
$E_1$	1.233	1.238
$H_1$	-0.065	-0.081
$H_2$	-0.088	-0.097
$H_2$	-0.094	-0.103
$H_4$	-0.105	-0.110

symmetries, respectively. The measured separation in energy is higher than the theoretical one, but such a difference is consistent with the fact that the potential applied between the tip and the sample does not completely drop only in the vacuum barrier but also in the semiconductor.<sup>31,32</sup> Regarding higher electron states, we observe that  $E_3$  slightly extends out of the dot in Fig. 2(b). However, variations in the localization of  $E_3$  are found from one dot to another, which indicates a small confinement for this state and thus a larger dependence of its extent on the fluctuations of the dot geometry and composition. It is also difficult to determine if we probe only one state or if the feature associated with  $E_3$  arises from the contribution of a few states since the energy separation between higher states becomes of the order of our spectral resolution. Furthermore, we cannot guarantee that the cleavage occurs right at the center of the dot, leaving some uncertainty about the extent of the second electron excited state.

In contrast, an inspection of the hole localization reveals strong differences between the experimental observations and the theoretical calculations, which already occur for the ground state. From the calculations of the electronic structure, this state is found to be slightly localized toward the top of the dot due to the higher In composition in this region, thus giving rise to a small dipole moment. However, in all of the dots that were examined, we never observe such a localization, while the calculations clearly show that the cleavage of the dot does not affect the vertical localization of the ground state. Rather, the empty states we probe below the electron ground state are found at the interface between the dot and the capping layer. In addition, the energy separation that is measured between some peaks is of the order of the energy separation found for the electron states, whereas the theoretical hole level splittings are much smaller. Because the calculated hole localization is not shifted toward the QD interface by variations of the structural properties of the dots, it is difficult to attribute these interfacial states to the highest hole states of the dots.

Since more peaks are resolved in the tunneling spectra acquired at variable tip-sample distances below the electron

ground state than in the measurement performed at constant tip-sample distances, we cannot rule out a lack of sensitivity to detect the highest hole states in the latter case. However, none of our theoretical calculations shows holes trapped at the interface, at least for the eight first hole states. We also note that the lowest empty states are generally obtained at energies above +0.8 eV. If these states belong to the valence band of the QD, the tip Fermi level is not in resonance with the states when they are filled with tip electrons. Such result suggests the occurrence of inelastic processes in the tunneling of the electrons from the tip before they recombine with holes in the valence band. These processes might involve intermediate states, such as deep level states associated with point defects. Point defects have indeed been recently detected by low energy positron beam in the GaAs cap layer above the QDs.<sup>33</sup> While such defect states do not alter the optical properties of the embedded dots, surface effects due to the cleavage of the dot could modify the interaction between the deep levels and the dot valence band electronic structure.

## V. CONCLUSION

In conclusion, we have studied carrier transport through InAs/GaAs self-assembled QDs by scanning tunneling spectroscopy at low temperatures. The lowest electron states are found to be localized in the dot, and the symmetry of the ground and first excited states corresponds to those predicted by the tight-binding calculations of the QD single particle electronic structure. Empty states with lower energy are also observed with a surprising spatial distribution at the top interface of the dot. Because theoretical predictions of the valence band electronic structure do not show a significant modification of the hole localization along the growth direction between an embedded dot and a cleaved dot, further investigations are needed to understand the reproducible occurrence of states at the interface between the QDs and the GaAs capping layer.

<sup>1</sup>D. Bimberg, M. Grundmann, and N. N. Ledentsov, *Quantum Dot Heterostructures* (Wiley, Chichester, 1999).

<sup>2</sup>M. Henini, *Nanoscale Res. Lett.* **1**, 32 (2006).

<sup>3</sup>J. -Y. Marzin, J. -M. Gérard, A. Izraël, D. Barrier, and G. Bastard, *Phys. Rev. Lett.* **73**, 716 (1994).

<sup>4</sup>P. W. Fry, I. E. Itskevich, D. J. Mowbray, M. S. Skolnick, J. J. Finley, J. A. Barker, E. P. O'Reilly, L. R. Wilson, I. A. Larkin, P. A. Maksym, M. Hopkinson, M. Al-Khafaji, J. P. R. David, A. G. Cullis, G. Hill, and J. C. Clark, *Phys. Rev. Lett.* **84**, 733 (2000).

<sup>5</sup>G. Bester and A. Zunger, *Phys. Rev. B* **71**, 045318 (2005).

<sup>6</sup>L. He, G. Bester, and A. Zunger, *Phys. Rev. B* **70**, 235316 (2004).

<sup>7</sup>D. V. Regelman, D. Gershoni, E. Ehrenfreund, W. V. Shoenfeld, and P. M. Petroff, *Physica E (Amsterdam)* **13**, 114 (2002).

<sup>8</sup>E. E. Vdovin, A. Levin, A. Patanè, L. Eaves, P. C. Main, Yu. N. Khanin, Yu. V. Dubrovskii, M. Henini, and G. Hill, *Science* **290**, 122 (2000).

<sup>9</sup>B. Grandidier, Y. M. Niquet, B. Legrand, J. P. Nys, C. Priester, D. Stiévenard, J. M. Gérard, and V. Thierry-Mieg, *Phys. Rev. Lett.* **85**, 1068 (2000).

<sup>10</sup>O. Millo, D. Katz, Y. Cao, and U. Banin, *Phys. Rev. Lett.* **86**, 5751 (2001).

<sup>11</sup>T. Maltezopoulos, A. Bolz, C. Meyer, C. Heyn, W. Hansen, M. Morgenstern, and R. Wiesendanger, *Phys. Rev. Lett.* **91**, 196804 (2003).

<sup>12</sup>T. K. Johal, R. Rinaldi, A. Passaseo, R. Cingolani, A. Vasanelli, R. Ferreira, and G. Bastard, *Phys. Rev. B* **66**, 075336 (2002).

<sup>13</sup>P. Kailuweit, D. Reuter, A. D. Wieck, O. Wibbelhoff, A. Lorke, U. Zeitler, and J. C. Maan, *Physica E (Amsterdam)* **32**, 159 (2006).

<sup>14</sup>D. Reuter, P. Kailuweit, R. Roescu, A. D. Wieck, O. Wibbelhoff, A. Lorke, U. Zeitler, and J. C. Maan, *Phys. Status Solidi B* **243**, 3942 (2006).

<sup>15</sup>A. Patanè, R. J. A. Hill, L. Eaves, P. C. Main, M. Henini, M. L.

- Zambrano, A. Levin, N. Mori, C. Hamaguchi, Yu. V. Dubrovskii, E. E. Vdovin, D. G. Austing, S. Tarucha, and G. Hill, *Phys. Rev. B* **65**, 165308 (2002).
- <sup>16</sup>B. Legrand, J. P. Nys, B. Grandidier, D. Stiévenard, A. Lemaitre, J. M. Gérard, and V. Thierry-Mieg, *Appl. Phys. Lett.* **74**, 2608 (1999).
- <sup>17</sup>O. Flebbe, H. Eisele, T. Kalka, F. Heinrichsdorff, A. Krost, D. Bimberg, and M. Dähne-Priestch, *J. Vac. Sci. Technol. B* **17**, 1639 (1999).
- <sup>18</sup>LT-STM Omicron Nanotechnology.
- <sup>19</sup>A. Lemaître, G. Patriarche, and F. Glas, *Appl. Phys. Lett.* **85**, 3717 (2004).
- <sup>20</sup>P. Mårtensson and R. M. Feenstra, *Phys. Rev. B* **39**, 7744 (1989).
- <sup>21</sup>G. Mahieu, B. Grandidier, D. Deresmes, J. P. Nys, D. Stiévenard, and Ph. Ebert, *Phys. Rev. Lett.* **94**, 026407 (2005).
- <sup>22</sup>D. Reuter, P. Kailuweit, A. D. Wieck, U. Zeitler, O. Wibbelhoff, C. Meier, A. Lorke, and J. C. Maan, *Phys. Rev. Lett.* **94**, 026808 (2005).
- <sup>23</sup>W.-H. Chang, W. Y. Chen, T. M. Hsu, N.-T. Yeh, and J.-I. Chyi, *Phys. Rev. B* **66**, 195337 (2002).
- <sup>24</sup>J. Mysliveček, A. Stróžecka, J. Steffl, P. Sobotík, I. Ošťádal, and B. Voigtländer, *Phys. Rev. B* **73**, 161302(R) (2006).
- <sup>25</sup>T. Soubiron, R. Stiufiuc, L. Patout, D. Deresmes, B. Grandidier, and D. Stiévenard, *Appl. Phys. Lett.* **90**, 102112 (2007).
- <sup>26</sup>A. J. Williamson, L. W. Wang, and A. Zunger, *Phys. Rev. B* **62**, 12963 (2000).
- <sup>27</sup>S.-H. Wei and A. Zunger, *Phys. Rev. B* **60**, 5404 (1999).
- <sup>28</sup>L.-W. Wang, J. Kim, and A. Zunger, *Phys. Rev. B* **59**, 5678 (1999).
- <sup>29</sup>J.-M. Jancu, R. Scholz, F. Beltram, and F. Bassani, *Phys. Rev. B* **57**, 6493 (1998).
- <sup>30</sup>C. C. G. Van de Walle, *Phys. Rev. B* **39**, 1871 (1989).
- <sup>31</sup>G. Medeiros-Ribeiro, D. Leonard, and P. M. Petroff, *Appl. Phys. Lett.* **66**, 1767 (1995).
- <sup>32</sup>P. Liljeroth, P. A. Zeijlmans van Emmichoven, S. G. Hickey, H. Weller, B. Grandidier, G. Allan, and D. Vanmaekelbergh, *Phys. Rev. Lett.* **95**, 086801 (2005).
- <sup>33</sup>X. Q. Meng, Z. Q. Chen, P. Jin, Z. G. Wang, and L. Wei, *Appl. Phys. Lett.* **91**, 093510 (2007).